Cross sections for valence-shell excitations of H_2O in the 9.85–12.15-eV energy-loss range studied by high-energy inelastic electron scattering

Wei-Qing Xu,[2,*] Yi-Geng Peng,[3,4,*] Jian-Hui Zhu,[1,*] Xiao-Jiao Du,[1] Yuan-Chen Xu,[1] Li-Han Wang,[1] Bo Li,[1] Hao-Ran Zhang,[1] Bei-Yuan Zhang,[1] Zi-Ru Ma,[1] Shu-Xing Wang,[1] Yong Wu,[4,5,†] Jian-Guo Wang,[4] and Lin-Fan Zhu[1,‡]

[1]*Hefei National Laboratory for Physical Sciences at Microscale and Department of Modern Physics, University of Science and Technology of China, Hefei, Anhui 230026, China*

[2]*Center for Transformative Science, ShanghaiTech University, Shanghai 201210, China*

[3]*Department of Applied Physics, Nanjing University of Science and Technology, Nanjing 210094, China*

[4]*Institute of Applied Physics and Computational Mathematics, Beijing 100088, China*

[5]*HEDPS, Center for Applied Physics and Technology, and College of Engineering, Peking University, Beijing 100871, China*

(Received 25 October 2021; accepted 17 February 2022; published 4 March 2022)

The recent measurement of the generalized oscillator strengths (GOSs) for $\tilde{A}\ ^1B_1$ and $\tilde{B}\ ^1A_1$ of H_2O exhibits the apparent deviations from the first Born approximation calculations in the large squared momentum transfer region [W. Q. Xu *et al.*, Phys. Rev. A **103**, 032808 (2021)]. Here a simplified theoretical model was proposed to calculate the GOSs of the two excitations at large momentum transfer within the second Born approximation. The accord of the experimental GOSs and the theoretical ones is improved, but the differences still exist. In addition, the GOSs and the integral cross sections for the higher excitations of H_2O in 9.85–12.15 eV are presented, which could be used to complete the database of electron-impact excitation cross sections of H_2O and be beneficial for modeling interaction processes between electrons and H_2O in the earth's atmosphere, plasmas, radiation physics, biology, etc.

DOI: 10.1103/PhysRevA.105.032801

I. INTRODUCTION

The significant disagreements of generalized ossillator strengths (GOSs) for electron-impact excitations of small systems between the accurate calculations within the first Born approximation (FBA) and the high-precision measurements in the large-momentum-transfer K region have puzzled the related community for decades [1–6]. The works of Bradley *et al.* on N_2 [7] and Zhu *et al.* on Ne [8] have concluded that the discrepancies are due to the high-order Born term (or termed as intramolecular multiple scattering [7]), wherein they employed a new experimental technique, i.e., nonresonant inelastic x-ray scattering, to probe the same physical quantity as inelastic electron scattering but whose scattering dynamics obey the lowest-order theoretical approaches. Recently, we made a joint experimental and theoretical investigation on the electron-impact excitations $\tilde{A}\ ^1B_1$ and $\tilde{B}\ ^1A_1$ of H_2O, and a similar phenomenon of the obvious GOS deviation of high-energy electron scattering results from FBA calculations in the large K^2 region was observed [9]. By taking into account the second Born term, herein we reinvestigate the GOS behaviors of $\tilde{A}\ ^1B_1$ and $\tilde{B}\ ^1A_1$ of H_2O. In addition, the previous works about the GOSs and the integral cross sections (ICSs) for valence-shell excitations of H_2O focus on the low-energy excitations below ∼10 eV both experimentally [2,9–15] and theoretically [11,12,16,17] (e.g., see Ref. [9]), while the higher excitations with abundant vibronic structures are investigated to a lesser extent [10,16]. The photoabsorption cross sections and the optical oscillator strengths (OOSs) for the excitations above ∼10 eV were measured by photoabsorption [18–24] and dipole (e, e) [25–27] methods.

In this paper, we propose a simplified theoretical model to calculate the GOSs for $\tilde{A}\ ^1B_1$ and $\tilde{B}\ ^1A_1$ of H_2O in the large K^2 region within the second Born approximation (SBA) by the multireference single- and double-excitation configuration interaction method (MRD-CI), and we compare them with the reported experimental ones measured by high-energy electron scattering [9]. In addition, the GOSs and ICSs of the higher excitations of H_2O in 9.85–12.15 eV are also presented. The experimental apparatus and procedures are described in Sec. II, theoretical details are given in Sec. III, and the results are presented and discussed in Sec. IV.

II. EXPERIMENTAL APPARATUS AND PROCEDURES

The high-resolution electron-energy-loss spectrometer and experimental procedures have been described in detail in Refs. [9,28]. Briefly, the electron energy was set at 1500 eV with an energy resolution of about 70 meV (full width at half maximum, FWHM), and the standard relative flow technique [29], was utilized to determine absolute differential cross sections (DCSs) for electronic excitations of H_2O with a standard sample of helium used. The electron-energy-loss spectra in the angular range of 1.5°−9.0° with an angular

*These authors contributed equally to this work.
†wu_yong@iapcm.ac.cn
‡lfzhu@ustc.edu.cn

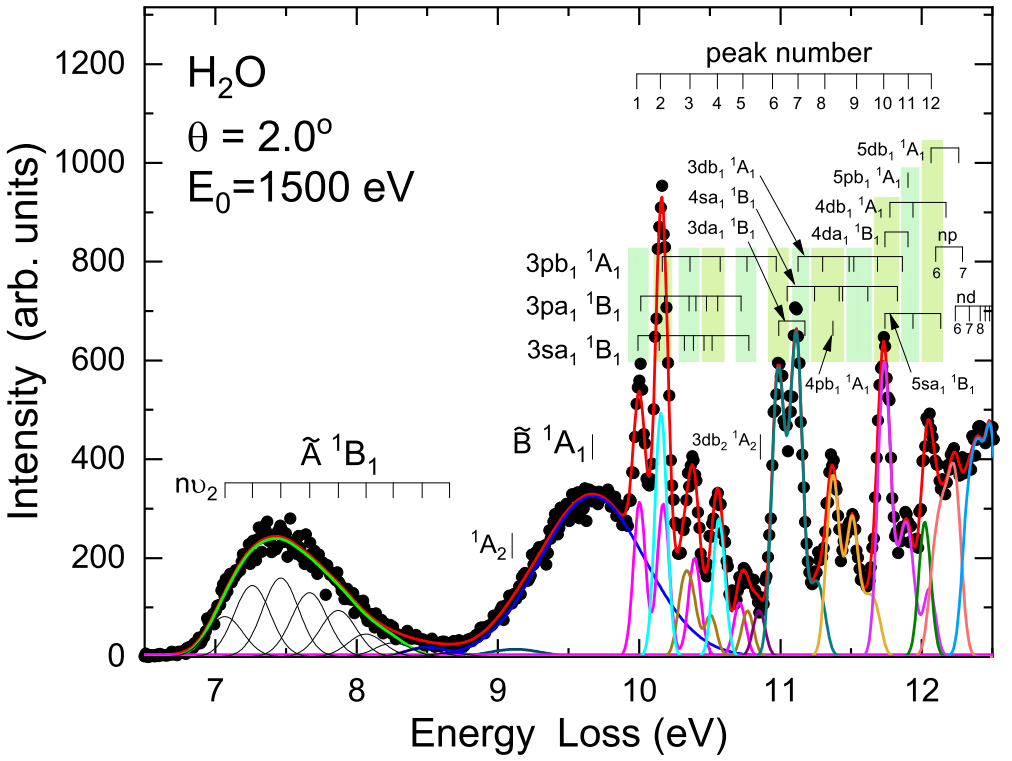

FIG. 1. A typical EELS of H_2O at an incident electron energy of 1500 eV and a scattering angle of 2.0°. Solid lines are the fitted curves. The 12 numbers in the top right corner label the peaks above 9.85 eV, and the shadow bands show the corresponding contributed transitions listed in Table I (see text for details).

resolution of about 0.8° (FWHM) were measured, and the angular intervals are 0.5° for 1.5°−5.5° and 1.0° for 6°−9°, respectively. The DCS $d\sigma_{H_2O}/d\Omega$ of a specified excitation with an excitation energy E_n of H_2O can be determined from the measured electron-energy-loss spectrum (EELS) by referring to the DCS $d\sigma_{He}/d\Omega$ of $1s^2\ ^1S_0 \rightarrow 1s2p\ ^1P_1$ (E_{2p}) of He at a scattering angle θ [29]:

$$\frac{d\sigma_{H_2O}(E_n,\theta)}{d\Omega} = \frac{\dot{n}_{He}}{\dot{n}_{H_2O}}\sqrt{\frac{M_{He}}{M_{H_2O}}}\frac{N_{H_2O}(E_n,\theta)}{N_{He}(E_{2p},\theta)}\frac{d\sigma_{He}(E_{2p},\theta)}{d\Omega}, \tag{1}$$

where $\dot{n}$ represents the flow rate, and N refers to the intensity of the corresponding excitation. M is the molecular mass for the specified molecule. The $d\sigma_{He}(E_{2p},\theta)/d\Omega$ of He has been determined with a high accuracy [30].

Figure 1 shows a typical EELS of H_2O at $E_0 = 1500$ eV and $\theta = 2.0°$ with spectroscopic assignments according to Refs. [10,18,24,31,32]. In order to determine the intensities of the features of H_2O, the nonlinear least-squares fitting method was used to fit the measured spectra. The natures of the profiles of $\tilde{A}\ ^1B_1$, $\tilde{B}\ ^1A_1$, and $^1A_2$ have been described in detail in our recent paper [9], where $\tilde{A}\ ^1B_1$ was depicted by nine Gaussian functions for individual vibronic states as shown in Fig. 1. $\tilde{B}\ ^1A_1$ was fitted with a Gaussian function ($E_n = 9.67$ eV, $\Delta E = 0.88$ eV), and $^1A_2$ was also represented by a Gaussian function ($E_n = 9.12$ eV, $\Delta E = 0.43$ eV). Herein we look into the higher excitations in the range of 9.85–12.5 eV. The Gaussian functions with the same width were used to depict the profiles of the three vibrational series of $3pb_1\ ^1A_1$, $3pa_1\ ^1B_1$, and $3sa_1\ ^1B_1$, where the corresponding energy positions were fixed to the ones in Tables 3 and 4 of Ref. [18]. The vibronic states in the range of 11–12.5 eV [10,18,24,31,32] were also modeled by Gaussian functions with the same width as the above three vibrational series. Due to the serious overlapping among the excitations in the range of 9.85–12.5 eV, the random intensity allocations among them may result in large experimental errors. So we labeled 12 peaks, shown in Fig. 1 and listed in Table I, where the contributed intensities from the excitations for the corresponding peaks were summed to determine the total DCSs of these excitations. The presently determined DCSs are listed in Table II.

According to the FBA, the GOS $f(E_n,\mathbf{K})$ can be written as (in atomic units) [1]

$$f(E_n,\mathbf{K}) = \frac{E_n}{2}\frac{p_0}{p_a}K^2\frac{d\sigma(E_n,\theta)}{d\Omega}, \tag{2}$$

where p_0 and p_a are the incident and scattered electron momenta, respectively; $\mathbf{K}$ is the corresponding momentum transfer vector at θ; and $\mathbf{K^2}$ is the momentum transfer squared. The presently determined GOSs are listed in Table III.

In addition, according to the analytic properties of the GOS identified by Lassettre and his coworkers [33,34], the GOS can be represented by [33–36]

$$f(E_n,\mathbf{K}) = \frac{x^M}{(1+x)^{l+l'+M+5}}\sum_{m=0}^{\infty}\frac{f_m x^m}{(1+x)^m}, \tag{3}$$

where $x = K^2/\alpha^2$, with $\alpha = (2I)^{1/2} + [2(I-E_n)]^{1/2}$ and I being the ionization energy. l and l' are the orbital angular

TABLE I. The contributed transitions for the corresponding peaks labeled in Fig. 1.

Peak number	Transitions
1	$3sa_1\ ^1B_1(000) + 3pa_1\ ^1B_1(000)$
2	$3sa_1\ ^1B_1(010) + 3pa_1\ ^1B_1(010) + 3pb_1\ ^1A_1(000)$
3	$3sa_1\ ^1B_1(020, 100) + 3pa_1\ ^1B_1(020, 100) + 3pb_1\ ^1A_1(010)$
4	$3sa_1\ ^1B_1(030, 110) + 3pa_1\ ^1B_1(030, 110) + 3pb_1\ ^1A_1(020)$
5	$3sa_1\ ^1B_1(200) + 3pa_1\ ^1B_1(120) + 3pb_1\ ^1A_1(030)$
6	$3pb_1\ ^1A_1(200) + 3da_1\ ^1B_1(000) + 4sa_1\ ^1B_1(000)$
7	$3da_1\ ^1B_1(010) + 3db_1\ ^1A_1(000)$
8	$3db_1\ ^1A_1(010) + 4sa_1\ ^1B_1(010, 020, 100) + 4pb_1\ ^1A_1$
9	$3db_1\ ^1A_1(020, 100) + 4sa_1\ ^1B_1(110)$
10	$3db_1\ ^1A_1(110) + 4sa_1\ ^1B_1(200) + 4da_1\ ^1B_1(000) + 4db_1\ ^1A_1(000) + 5sa_1\ ^1B_1(000)$
11	$3db_1\ ^1A_1(120) + 4da_1\ ^1B_1(010) + 4db_1\ ^1A_1(010) + 5pb_1\ ^1A_1 + 5sa_1\ ^1B_1(010)$
12	$5db_1\ ^1A_1(000) + 6p + 5sa_1\ ^1B_1(100)$

momenta of the initial and final states of the target electron, while M is an integer which is relevant to the transition multipolarity [35,36] and f_m are the fitting parameters. For a dipole-allowed transition, $M = 0$ and f_0 is the OOS. Since the ionization energy I of an electron in a molecule is defined only in the context of a simply independent particle model by Lassettre [33], it is better to simply take α^2 as a fitting parameter along with f_m as proposed by Kim [36]. Moreover, the following function $g(x)$ with two fitting parameters a and b, in addition to the leading fraction in Eq. (3), can well represent the experimental GOS:

$$g(x) = axe^{-bx}. \tag{4}$$

Similar treatments can be found in previous works [37].

From the fitted GOS results using the Lassettre formula [33–36], the Born ICSs for the electron-impact excitations can be calculated (in atomic units) [1] as follows:

$$\sigma_{\text{Born}}(E_0) = \frac{\pi}{E_0 E_n} \int_{K^2_{\text{min}}}^{K^2_{\text{max}}} \frac{f(E_n, \mathbf{K})}{K^2} dK^2, \tag{5}$$

with

$$K^2_{\text{min}} = [\sqrt{2E_0} - \sqrt{2(E_0 - E_n)}]^2$$

and

$$K^2_{\text{max}} = [\sqrt{2E_0} + \sqrt{2(E_0 - E_n)}]^2,$$

where K_{min} and K_{max} represent the minimum and maximum momentum transfers, respectively. However, σ_{Born} is generally overestimated at low and intermediate energies [2]. Therefore, Kim developed a BE-scaling (B is the binding energy and E is the excitation energy) approach to scale σ_{Born} into the BE-scaled ICS [2,38],

$$\sigma_{\text{BE}}(E_0) = \frac{E_0}{E_0 + B + E_n} \sigma_{\text{Born}}(E_0), \tag{6}$$

which can correct the deficiency of the FBA at low E_0, without losing its well-known validity at high E_0. Here B is the binding energy. The reliability of this method and the high accuracy of σ_{BE} have been widely attested by numerous experiments and theories [2,38].

The experimental errors of the GOSs in this work include the contributions from the finite angular resolution, the angle determination, the statistical counts, the fitting procedure, and the normalizing procedure, and the total experimental errors are shown in the corresponding figures in Sec. IV.

TABLE II. The DCSs for the labeled peaks shown in Fig. 1 and Table I (in units of $a_0^2\ sr^{-1}$). The numbers in square brackets denote the power of ten.

θ	1[a]	2[a]	3[a]	4[a]	5[a]	6[a]	7[a]	8[a]	9[a]	10[a]	11[a]	12[a]
1.5°	4.58[−1]	1.10	6.67[−1]	5.97[−1]	3.11[−1]	1.15	1.07	8.71[−1]	6.38[−1]	1.29	3.96[−1]	9.89[−1]
2°	2.79[−1]	7.15[−1]	3.83[−1]	3.32[−1]	1.80[−1]	5.83[−1]	5.60[−1]	5.29[−1]	3.19[−1]	6.55[−1]	2.91[−1]	5.43[−1]
2.5°	1.40[−1]	3.85[−1]	1.80[−1]	1.74[−1]	8.71[−2]	2.52[−1]	2.41[−1]	2.46[−1]	1.69[−1]	3.26[−1]	1.38[−1]	2.87[−1]
3°	7.99[−2]	2.49[−1]	1.02[−1]	1.03[−1]	4.69[−2]	1.43[−1]	1.14[−1]	1.61[−1]	1.01[−1]	1.80[−1]	9.13[−2]	1.70[−1]
3.5°	4.72[−2]	1.59[−1]	5.79[−2]	6.44[−2]	2.96[−2]	7.84[−2]	6.34[−2]	1.07[−1]	5.67[−2]	1.01[−1]	6.78[−2]	1.06[−1]
4°	2.86[−2]	1.04[−1]	3.46[−2]	3.98[−2]	1.93[−2]	4.91[−2]	3.60[−2]	6.90[−2]	3.55[−2]	6.85[−2]	3.91[−2]	7.17[−2]
4.5°	1.52[−2]	5.95[−2]	1.81[−2]	2.24[−2]	1.06[−2]	2.38[−2]	1.96[−2]	3.85[−2]	2.13[−2]	3.23[−2]	2.82[−2]	3.99[−2]
5°	7.90[−3]	3.75[−2]	1.06[−2]	1.41[−2]	6.67[−3]	1.48[−2]	1.10[−2]	2.50[−2]	1.43[−2]	2.08[−2]	1.81[−2]	2.30[−2]
5.5°	4.62[−3]	2.34[−2]	6.34[−3]	9.03[−3]	4.19[−3]	9.29[−3]	6.70[−3]	1.58[−2]	9.68[−3]	1.32[−2]	1.12[−2]	1.34[−2]
6°	2.42[−3]	1.41[−2]	3.61[−3]	5.42[−3]	2.72[−3]	5.57[−3]	3.96[−3]	8.95[−3]	5.66[−3]	8.07[−3]	6.46[−3]	8.13[−3]
7°	8.09[−4]	6.29[−3]	1.49[−3]	2.76[−3]	1.36[−3]	2.88[−3]	1.63[−3]	3.72[−3]	2.89[−3]	3.05[−3]	3.21[−3]	4.11[−3]
8°	7.78[−4]	4.11[−3]	1.25[−3]	2.06[−3]	1.06[−3]	1.61[−3]	8.45[−4]	2.17[−3]	1.86[−3]	1.85[−3]	1.90[−3]	2.33[−3]
9°	1.02[−3]	3.51[−3]	1.23[−3]	1.83[−3]	8.03[−4]	1.10[−3]	9.18[−4]	1.90[−3]	1.33[−3]	1.76[−3]	1.52[−3]	1.64[−3]

[a]The numbers here correspond to the labeled peaks shown in Fig. 1 and Table I.

TABLE III. The derived GOSs according to the corresponding DCSs listed in Table II (in atomic units). The numbers in square brackets denote the power of ten.

K^2	1[a]	2[a]	3[a]	4[a]	5[a]	6[a]	7[a]	8[a]	9[a]	10[a]	11[a]	12[a]
0.00	8.45[−3]	1.83[−2]	1.37[−2]	9.74[−3]	6.27[−3]	2.66[−2]	2.51[−2]	1.76[−2]	1.34[−2]	2.89[−2]	7.81[−3]	2.10[−2]
0.08	6.81[−3]	1.66[−2]	1.03[−2]	9.34[−3]	4.98[−3]	1.89[−2]	1.78[−2]	1.48[−2]	1.10[−2]	2.27[−2]	7.06[−3]	1.79[−2]
0.13	6.90[−3]	1.80[−2]	9.81[−3]	8.63[−3]	4.79[−3]	1.59[−2]	1.54[−2]	1.49[−2]	9.12[−3]	1.91[−2]	8.59[−3]	1.63[−2]
0.22	5.63[−3]	1.58[−2]	7.53[−3]	7.37[−3]	3.77[−3]	1.12[−2]	1.08[−2]	1.13[−2]	7.85[−3]	1.55[−2]	6.61[−3]	1.40[−2]
0.31	4.51[−3]	1.43[−2]	5.99[−3]	6.14[−3]	2.84[−3]	8.88[−3]	7.16[−3]	1.03[−2]	6.59[−3]	1.20[−2]	6.14[−3]	1.16[−2]
0.41	3.53[−3]	1.21[−2]	4.49[−3]	5.07[−3]	2.38[−3]	6.45[−3]	5.28[−3]	9.12[−3]	4.89[−3]	8.89[−3]	6.04[−3]	9.64[−3]
0.52	2.75[−3]	1.02[−2]	3.45[−3]	4.03[−3]	2.00[−3]	5.20[−3]	3.87[−3]	7.57[−3]	3.95[−3]	7.77[−3]	4.49[−3]	8.37[−3]
0.67	1.88[−3]	7.48[−3]	2.33[−3]	2.92[−3]	1.41[−3]	3.23[−3]	2.70[−3]	5.42[−3]	3.04[−3]	4.70[−3]	4.16[−3]	5.98[−3]
0.85	1.24[−3]	5.98[−3]	1.73[−3]	2.33[−3]	1.13[−3]	2.56[−3]	1.93[−3]	4.47[−3]	2.59[−3]	3.83[−3]	3.38[−3]	4.37[−3]
1.00	8.53[−4]	4.38[−3]	1.21[−3]	1.75[−3]	8.32[−4]	1.89[−3]	1.38[−3]	3.32[−3]	2.06[−3]	2.87[−3]	2.47[−3]	3.00[−3]
1.21	5.41[−4]	3.20[−3]	8.35[−4]	1.27[−3]	6.52[−4]	1.37[−3]	9.84[−4]	2.27[−3]	1.46[−3]	2.12[−3]	1.72[−3]	2.20[−3]
1.66	2.47[−4]	1.96[−3]	4.71[−4]	8.89[−4]	4.46[−4]	9.67[−4]	5.56[−4]	1.29[−3]	1.02[−3]	1.10[−3]	1.17[−3]	1.52[−3]
2.19	3.14[−4]	1.69[−3]	5.23[−4]	8.72[−4]	4.59[−4]	7.16[−4]	3.79[−4]	9.98[−4]	8.65[−4]	8.80[−4]	9.15[−4]	1.14[−3]
2.74	5.18[−4]	1.80[−3]	6.45[−4]	9.75[−4]	4.37[−4]	6.12[−4]	5.17[−4]	1.10[−3]	7.74[−4]	1.05[−3]	9.14[−4]	1.01[−3]

[a]The numbers here correspond to the labeled peaks shown in Fig. 1 and Table I.

III. THEORETICAL METHOD

To explore the behaviors of the GOSs for $\tilde{A}\ ^1B_1$ and $\tilde{B}\ ^1A_1$ of H_2O in the large K range, the second Born term has been introduced into the inelastic electron-H_2O scattering calculation within the SBA by the MRD-CI. The MRD-CI has been applied to calculate the adiabatic potential curves and wave functions of the ground and excited states based on the Born-Oppenheimer approximation, which accurately deals with the influence of electron correlation on the related wave functions [9,39]. The electron-impact DCS $d\sigma/d\Omega$ for a specified excitation from an initial state i to a final state f of an atom or a molecule within the Born approximation is [1,2,40]

$$\frac{d\sigma}{d\Omega} = \frac{k_f}{k_i}|f_B|^2 = \frac{k_f}{k_i}\left|\sum_{n=1}^{\infty} f_{Bn}\right|^2. \tag{7}$$

Here f_B is the scattering amplitude, f_{Bn} is the nth scattering amplitude, and k_i and k_f are the incident and scattered electron momenta, respectively. For electron-molecule collision, the first Born scattering amplitude is

$$f_{B1} = -\frac{2}{K^2}\left[F_{fi}(\mathbf{K}) - \delta_{fi}\sum_{\alpha} Z_\alpha e^{i\mathbf{K}\cdot\mathbf{R}_\alpha}\right], \tag{8}$$

with

$$F_{fi}(\mathbf{K}) = \langle f|\sum_j e^{i\mathbf{K}\cdot\mathbf{r}_j}|i\rangle.$$

Here $\mathbf{K} = \mathbf{k}_i - \mathbf{k}_f$ is the momentum transfer, and Z_α and $\mathbf{R}_\alpha$ are the nuclear charge and the position vector of the αth atom in the molecule target, respectively. F_{fi} is called the Born amplitude, and $\mathbf{r}_j$ is the position vector of the jth electron. δ_{fi} is the usual Kronecker symbol. Then, within the FBA, $f_B = f_{B1}$.

The second Born scattering amplitude is [5]

$$f_{B2} = -\sum_e \frac{2}{\pi^2}\lim_{\epsilon\to 0^+}\int d\mathbf{k}\ \frac{\mathscr{F}_{fe}(\mathbf{k}_f,\mathbf{k})\mathscr{F}_{ei}(\mathbf{k},\mathbf{k}_i)}{|\mathbf{k}_f-\mathbf{k}|^2|\mathbf{k}-\mathbf{k}_i|^2(k_e^2-k^2+i\epsilon)}, \tag{9}$$

with

$$\mathscr{F}_{mn}(\mathbf{k}_m,\mathbf{k}_n) = F_{mn}(\mathbf{k}_n-\mathbf{k}_m) - \delta_{mn}\sum_\alpha Z_\alpha e^{i(\mathbf{k}_n-\mathbf{k}_m)\cdot\mathbf{R}_\alpha},$$

$$F_{mn}(\mathbf{k}_n-\mathbf{k}_m) = \langle m|\sum_j e^{i(\mathbf{k}_n-\mathbf{k}_m)\cdot\mathbf{r}_j}|n\rangle.$$

Here $k_e^2 = k_i^2 - 2\omega_e$, and ω_e represents the excitation energy for the intermediate state of the target. The summation on the intermediate state e is over all bound and continuum states. So, within the SBA, $f_B = f_{B1} + f_{B2}$.

For the molecule target with free spatial orientation of the molecular axis in a practical experiment, the $d\sigma/d\Omega$ should be averaged by holding the molecular axis fixed and allowing $\mathbf{K}$ to change its relative orientation:

$$\frac{d\bar{\sigma}(\mathbf{K})}{d\Omega} = \frac{1}{4\pi}\int \frac{d\sigma(\mathbf{K})}{d\Omega}d\Omega_{\hat{K}}. \tag{10}$$

The numerical solution of f_{B1} is easy as long as the accurate electronic wave functions of the initial and final states are obtained. However, the infinite summation on e of f_{B2} in Eq. (9) makes an exact SBA calculation computationally prohibitive. Therefore, some kind of approximation is normally introduced. Note that f_{B2} has one first-order pole of $k = k_e$ on the real axis x of the complex plane z shown in Fig. 2; therefore, we can separate Eq. (9) into two parts as

$$f_{B2} = P_V + R_{es}, \tag{11}$$

with the principal value (P_V) integration part

$$P_V = -\sum_e \frac{2}{\pi^2}\lim_{\epsilon\to 0^+}\left[\int d\Omega\int_0^{k_e-\epsilon} k^2dk\ \frac{\mathscr{F}_{fei}(\mathbf{k}_f,\mathbf{k},\mathbf{k}_i)}{k_e^2-k^2+i\epsilon} + \int d\Omega\int_{k_e+\epsilon}^{\infty} k^2dk\ \frac{\mathscr{F}_{fei}(\mathbf{k}_f,\mathbf{k},\mathbf{k}_i)}{k_e^2-k^2+i\epsilon}\right], \tag{12}$$

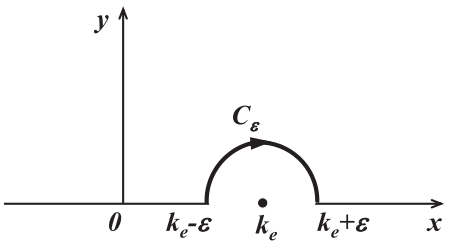

FIG. 2. The schematic diagram of the integral path on the complex plane z for f_{B2} in Eq. (9), where $k = k_e$ is the first-order pole on the real axis x (see text for details).

with

$$\mathscr{F}_{fei}(\mathbf{k}_f, \mathbf{k}, \mathbf{k}_i) = \frac{\mathscr{F}_{fe}(\mathbf{k}_f, \mathbf{k})\mathscr{F}_{ei}(\mathbf{k}, \mathbf{k}_i)}{|\mathbf{k}_i - \mathbf{k}|^2|\mathbf{k} - \mathbf{k}_f|^2},$$

and, according to the residue theorem, the residual (R_{es}) integration part

$$R_{es} = -\sum_e \frac{2}{\pi^2} \lim_{\epsilon\to 0^+} \int d\Omega \int_{C_\epsilon} z^2 dz \, \frac{\mathscr{F}_{fei}(\mathbf{k}_f, \mathbf{z}, \mathbf{k}_i)}{k_e^2 - z^2 + i\epsilon}$$
$$= \sum_e \frac{i}{\pi} \int d\Omega_{\hat{k}_e} \, k_e \mathscr{F}_{fei}(\mathbf{k}_f, \mathbf{k}_e, \mathbf{k}_i). \quad (13)$$

Looking at P_V in Eq. (12), the numerator of $\mathscr{F}_{fei}(\mathbf{k}_f, \mathbf{k}, \mathbf{k}_i)$ is convergent for real k, and generally P_V is negligible (see the calculation in Fig. 4). For example, Hu *et al*. [41] ignored the P_V term in the $(e, 2e)$ cross-section calculation within the distorted-wave Born approximation (DWBA), but good agreement was achieved with the experimental values.

For R_{es} in Eq. (13), the calculation difficulty is to sum up all possible intermediate states e as claimed above. Here we included three cases which mainly contribute to f_{B2} [8]: (i) a large-angle elastic scattering from the ground state with $k_e = k_i$ followed by a near "0" angle inelastic scattering (i.e., $\tilde{X}\ ^1A_1 \to \tilde{X}\ ^1A_1 \to \tilde{A}\ ^1B_1/\tilde{B}\ ^1A_1$); (ii) a near "0" angle inelastic scattering from the ground state followed by a large-angle elastic scattering with $k_e = k_f$ (i.e., $\tilde{X}\ ^1A_1 \to \tilde{A}\ ^1B_1/\tilde{B}\ ^1A_1 \to \tilde{A}\ ^1B_1/\tilde{B}\ ^1A_1$), and (iii) the processes excited from the ground state $\tilde{X}\ ^1A_1$ to the intermediate states $\tilde{B}\ ^1A_1/\tilde{A}\ ^1B_1/\ ^1A_2$ and finally to the final states $\tilde{A}\ ^1B_1/\tilde{B}\ ^1A_1$ (i.e., $\tilde{X}\ ^1A_1 \to \tilde{B}\ ^1A_1/\tilde{A}\ ^1B_1/\ ^1A_2 \to \tilde{A}\ ^1B_1/\tilde{B}\ ^1A_1$). This consideration is reasonable because the DCSs of elastic scattering at large angles are much higher than the DCSs of inelastic scattering at the same angles, and the DCSs of inelastic scattering at small angles (especially near 0) are maximal and decrease rapidly with angles increasing for the dipole-allowed transitions, especially for water molecules with a strong permanent dipole moment. The present model can be extended to other molecular targets.

The electronic wave functions of the initial, intermediate, and final states were calculated with a combined multiconfiguration self-consistent field (MCSCF) + MRD-CI approach. The Dunning's quadruple-zeta basis set (aug-cc-pvqz) [42] was set on each hydrogen and oxygen atom. The molecular orbits were optimized with the MCSCF method embedded in the MOLPRO package [43], and the core shell of oxygen was kept frozen and the active space was formed with the rest of the eight valence electrons on six active orbits. In the MRD-CI calculation [44], a set of configurations was selected as the reference and the final CI space was formed by single and double excitation on the reference space. In addition, the effects of the one-dimensional nuclear vibration on the GOSs for $\tilde{A}\ ^1B_1$ and $\tilde{B}\ ^1A_1$ of H_2O were ignored according to the discussion in Ref. [9].

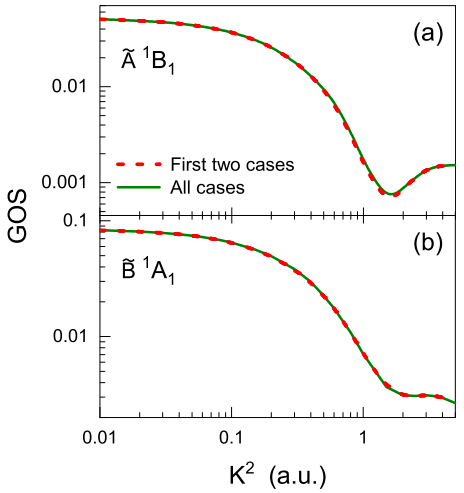

FIG. 3. The theoretical GOSs for (a) $\tilde{A}\ ^1B_1$ and (b) $\tilde{B}\ ^1A_1$ considering different intermediate processes. The red dashed line, "First two cases," indicates that "a large-angle elastic scattering from the ground state" plus "a near 0 angle inelastic scattering from the ground state" is included within the SBA calculations. The green solid line, "All cases," indicates the "first two cases" plus "$\tilde{X}\ ^1A_1 \to \tilde{B}\ ^1A_1/\tilde{A}\ ^1B_1/\ ^1A_2 \to \tilde{A}\ ^1B_1/\tilde{B}\ ^1A_1$" (see text for details).

IV. RESULTS AND DISCUSSION

A. The behaviors of GOSs for $\tilde{A}\ ^1B_1$ and $\tilde{B}\ ^1A_1$ in the large-momentum-transfer range

Figure 3 shows the calculated GOSs for $\tilde{A}\ ^1B_1$ and $\tilde{B}\ ^1A_1$ states considering different intermediate processes within the SBA by MRD-CI. It can been seen from Fig. 3 that the mentioned first two cases, i.e., "a large-angle elastic scattering from the ground state" plus "a near 0 angle inelastic scattering from the ground state" are dominant, while the third case, i.e., "$\tilde{X}\ ^1A_1 \to \tilde{B}\ ^1A_1/\tilde{A}\ ^1B_1/\ ^1A_2 \to \tilde{A}\ ^1B_1/\tilde{B}\ ^1A_1$" can be neglected. This confirms our simplified model mentioned above.

Figure 4 shows the theoretical GOSs for $\tilde{A}\ ^1B_1$ and $\tilde{B}\ ^1A_1$ with different calculation models by MRD-CI. The calculated GOSs between the FBA and the SBA for each state merge with each other in $K^2 < 0.2$ a.u. and rapidly diverge from one another in $K^2 > 1$ a.u. Moreover, it is shown in Fig. 4 that the differences of the GOSs with or without P_V within the SBA are very small for both states.

Figure 5 shows the present calculated GOSs for $\tilde{A}\ ^1B_1$ and $\tilde{B}\ ^1A_1$ of H_2O within the SBA by the MRD-CI compared with the previous FBA calculations [9,16] and measurements [9,13,14]. Very good agreement of the SBA-corrected GOSs with both the FBA calculation and the experimental GOSs of Xu *et al.* [9] in $K^2 < 0.5$ a.u. is expectedly observed. The discussion on the differences among the FBA calculations [9,16] and experimental values [9,13,14] has been detailed in

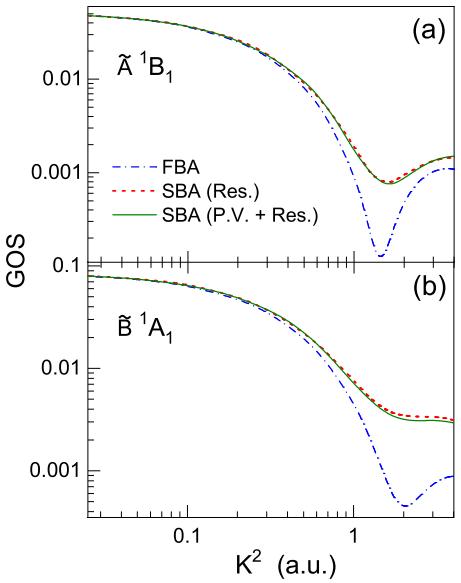

FIG. 4. The theoretical GOSs for (a) $\tilde{A}\ ^1B_1$ and (b) $\tilde{B}\ ^1A_1$ with different calculated models. Blue dash-dot lines are the calculated results within the first Born approximation (FBA) according to Eqs. (7), (8), and (10). Red dashed lines are the calculated results including only the residual integration part R_{es} of the second Born scattering amplitude f_{B2} within the second Born approximation (SBA) according to Eqs. (7), (10), (11), and (13). Green solid lines are the calculated results including both R_{es} and the principle value integration part P_V of f_{B2} within the SBA according to Eqs. (7) and (10)–(13) (see text for details).

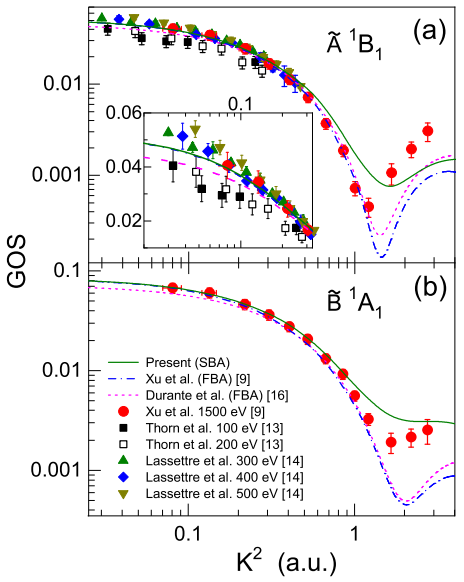

FIG. 5. The GOSs for (a) $\tilde{A}\ ^1B_1$ and (b) $\tilde{B}\ ^1A_1$, in comparison to different experimental results and calculations. Theory: Green solid lines are the present calculated results within the second Born approximation (SBA) according to Eqs. (7) and (10)–(13); blue dash-dot lines are the calculated results by Xu *et al.* [9] within the first Born approximation (FBA) according to Eqs. (7), (8), and (10); and magenta dashed lines are the calculated results by Durante *et al.* [16] within the FBA. Experiment: Red solid circles, Xu *et al.* [9] at $E_0 = 1500$ eV; black solid square and black open square, Thorn *et al.* [13] at $E_0 = 100$ and 200 eV, respectively; green solid upper triangle, blue solid rhombus, and dark yellow solid lower triangle, Lassettre and Skerbele [14] at $E_0 = 300$, 400, and 500 eV, respectively (see text for details).

Ref. [9]. Figure 5(a) shows the SBA-corrected GOSs of $\tilde{A}\ ^1B_1$ goes up in $K^2 > 0.5$ a.u. relative to the FBA ones of Xu *et al.* [9] by the MRD-CI and Durante *et al.* [16] by the random phase approximation (RPA), but the significant disagreement with the experimental GOSs of Xu *et al.* [9] in $K^2 > 0.68$ a.u. still exists in both magnitude and shape. Figure 5(b) shows the SBA-corrected GOSs of $\tilde{B}\ ^1A_1$ are in very good agreement with the experimental GOSs of Xu *et al.* [9] in $K^2 < 1$ a.u., while they are in qualitative agreement in $K^2 > 1$ a.u. with quantitative differences of about 20%–42%. In general, the present SBA-corrected GOSs improve the convergence between the experimental results [9] and the calculations within the FBA [9]. The existing discrepancies of the SBA calculations and the experimental results [9] could be due to the adopted simple SBA model, i.e., only three terms are used rather than the infinite summation over the intermediate states. So a more sophisticated model is needed to improve future calculations to explain the remaining differences, for example, considering more excited states and even continuous states in the intermediate state summation, and the contribution of higher-order Born terms.

B. The GOSs and ICSs for the excitations of H_2O in the range of 9.85–12.15 eV

Figure 6 shows the GOSs for the excitations of H_2O in the range of 9.85–12.15 eV, where the labeled numbers indicate the corresponding peaks shown in Fig. 1. The solid lines are the corresponding fitted results according to Eqs. (3) and (4). Generally, the GOSs show a similar behavior dependent on K^2, i.e., the GOSs decrease as K^2 increases and have a small increase at large K^2, which indicates a typical character of a dipole-allowed transition. Figure 7 shows the GOSs for the optically forbidden excitation $3db_2\ ^1A_2$ of H_2O, which show a similar behavior dependent on K^2 like the ones of dipole-allowed transitions in Fig. 6. This could be due to the weak intensity and heavy overlap with the fifth and sixth peaks as shown in Fig. 1. To the best of our knowledge, there are no other theoretical and experimental results to compare with the present GOSs.

Figure 8 shows the OOSs for the excitations of H_2O in the range of 9.85–12.15 eV by extrapolating the corresponding GOSs to the limit of $K^2 \to 0$, along with the previous measurements by photoabsorption [20–23] and dipole (e, e) [25] methods. It can be seen from Fig. 8 that the present OOSs are generally in good agreement with the photoabsorption ones [20,23] and the dipole (e, e) results [25] within the mutual experimental uncertainties. The present OOSs are in reasonable agreement with the ones of Smith *et al.* [21] and with the results of Rauk and Barriel [22] except for the second and sixth ones. The summation of the present OOSs is 0.1967, which is in good agreement with that of 0.1775 (by 10.82% larger) of Lee and Suto [20] within the experimental errors.

Figure 9 shows the BE-scaled ICSs for the excitations of H_2O in the range of 9.85–12.15 eV, where the ICSs for all

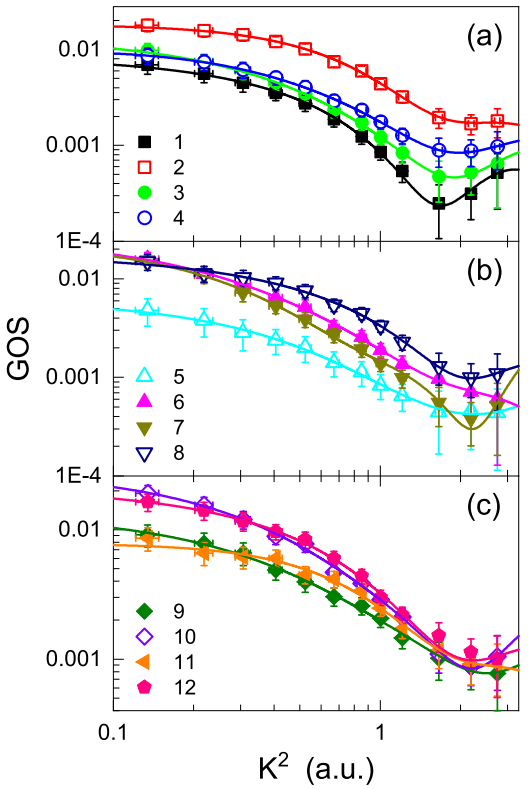

FIG. 6. The GOSs for the excitations of H_2O in the range of 9.85–12.15 eV. The labeled numbers in panels (a), (b), and (c) indicate the spectral peaks shown in Fig. 1 and Table I. Solid lines are the fitted GOSs of the corresponding peaks.

excitations first increase to the maxima and then decrease as the incident electron energy increases. Furthermore, it can be seen from Fig. 9 that the maximum positions of the ICSs are about 3–5 times the excitation energies, and the individual positions are related to the specific transitions. To the best of our knowledge, there are no other theoretical and experimental results to compare with the present ICSs. In fact, the electron-impact excitation ICS is one of the most widely used atomic and molecular parameters, but there is little research on it. The BE-scaling approach can give the credible ICSs in a wide energy range, which has been verified on many

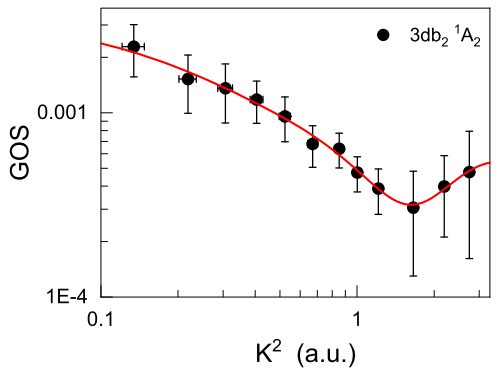

FIG. 7. The GOSs for $3db_2\ ^1A_2$ of H_2O, and the solid line is the fitted curve.

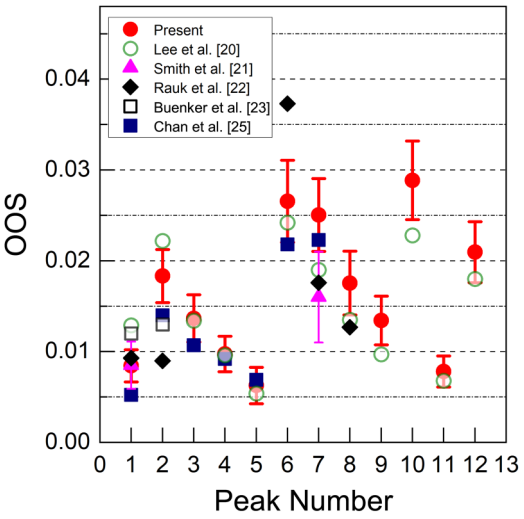

FIG. 8. The OOSs for the excitations of H_2O in the range of 9.85–12.15 eV. The peak numbers indicate the spectral peaks shown in Fig. 1 and Table I.

atoms and molecules [2,38]. Therefore, the BE-scaled ICSs given in this work are helpful to compile a complete database to improve the basic physical data of electron-H_2O interaction.

V. CONCLUSION

A simplified theoretical model within the SBA was proposed to explore the differences of the recently measured

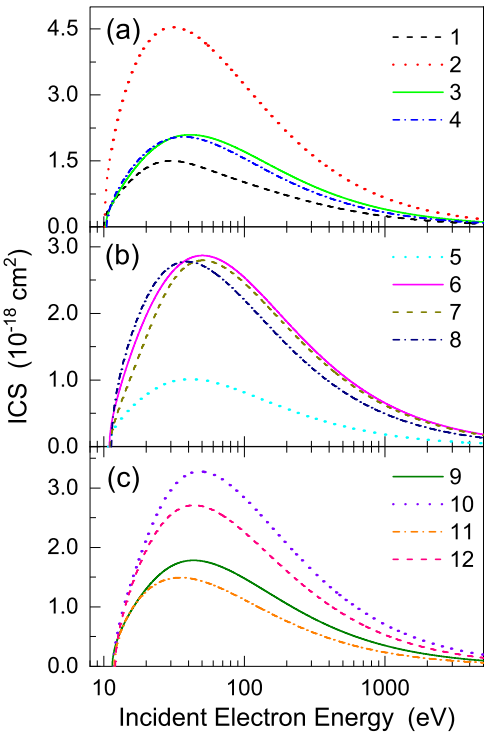

FIG. 9. The ICSs for the excitations of H_2O in the range of 9.85–12.15 eV. The labeled numbers in panels (a), (b), and (c) indicate the spectral peaks shown in Fig. 1 and Table I.

GOSs [9] for $\tilde{A}\ ^1B_1$ and $\tilde{B}\ ^1A_1$ of H_2O with the theoretical ones [9,16] within the FBA at large K^2. The agreement of the present calculated SBA GOSs and the measured ones [9] is better, but differences still exist, which calls for more theoretical work on this important issue. In addition, the GOSs and BE-scaled ICSs for the excitations of H_2O in the range of 9.85–12.15 eV are also obtained with the aid of the BE-scaling approach. This work would stimulate more in-depth and extensive research on this subject and would be helpful for modeling interaction processes between electrons and water-containing systems in planetary atmospheres, plasmas, radiation chemistry, and biology and biomedicine.

ACKNOWLEDGMENTS

This work was supported by the National Natural Science Foundation of China (Grants No. U1932207, No. 12174259, and No. 11604003), the National Key Research and Development Program of China (Grant No. 2017YFA0303500), and the Heavy Ion Research Facility in Lanzhou (HIRFL). W.-Q. Xu also acknowledges the support from the Shanghai-XFEL beamline project (SBP), the Shanghai Municipal Science and Technology Major Project (Grant No. 2017SHZDZX02), and the ShanghaiTech University High Performance Computing Public Service Platform.

[1] M. Inokuti, Rev. Mod. Phys. **43**, 297 (1971).
[2] H. Tanaka, M. J. Brunger, L. Campbell, H. Kato, M. Hoshino, and A. R. P. Rau, Rev. Mod. Phys. **88**, 025004 (2016).
[3] W.-B. Li, L.-F. Zhu, X.-J. Liu, Z.-S. Yuan, J.-M. Sun, H.-D. Cheng, Z.-P. Zhong, and K.-Z. Xu, Phys. Rev. A **67**, 062708 (2003); H. D. Cheng, L. F. Zhu, Z. S. Yuan, X. J. Liu, J. M. Sun, W. C. Jiang, and K. Z. Xu, *ibid.* **72**, 012715 (2005); L. F. Zhu, H. D. Cheng, Z. S. Yuan, X. J. Liu, J. M. Sun, and K. Z. Xu, *ibid.* **73**, 042703 (2006); C. B. Opal and E. C. Beaty, J. Phys. B **5**, 627 (1972); X. W. Fan and K. T. Leung, Phys. Rev. A **62**, 062703 (2000).
[4] Y.-K. Kim, M. Inokuti, G. E. Chamberlain, and S. R. Mielczarek, Phys. Rev. Lett. **21**, 1146 (1968).
[5] I. L. de Carvalho, J. Phys. B: At., Mol. Opt. Phys. **25**, 1287 (1992); **26**, 2179 (1993).
[6] S. Geltman and M. B. Hidalgo, J. Phys. B **4**, 1299 (1971); R. A. Bonham, J. Electron Spectrosc. Relat. Phenom. **3**, 85 (1974); M. Y. Amusia, L. V. Chernysheva, Z. Felfli, and A. Z. Msezane, Phys. Rev. A **67**, 022703 (2003); **75**, 062703 (2007); Z. F. Chen and A. Z. Msezane, J. Phys. B: At., Mol. Opt. Phys. **33**, 5397 (2000); E. J. Kelsey, Ann. Phys. (N.Y.) **322**, 1925 (2007).
[7] J. A. Bradley, G. T. Seidler, G. Cooper, M. Vos, A. P. Hitchcock, A. P. Sorini, C. Schlimmer, and K. P. Nagle, Phys. Rev. Lett. **105**, 053202 (2010).
[8] L. F. Zhu, W. Q. Xu, K. Yang, Z. Jiang, X. Kang, B. P. Xie, D. L. Feng, N. Hiraoka, and K. D. Tsuei, Phys. Rev. A **85**, 030501(R) (2012).
[9] W.-Q. Xu, Z.-R. Ma, Y.-G. Peng, X.-J. Du, Y.-C. Xu, L.-H. Wang, B. Li, H.-R. Zhang, B.-Y. Zhang, J.-H. Zhu, S.-X. Wang, Y. Wu, J.-G. Wang, and L.-F. Zhu, Phys. Rev. A **103**, 032808 (2021).
[10] Y. Itikawa and N. Mason, J. Phys. Chem. Ref. Data **34**, 1 (2005).
[11] K. Ralphs, G. Serna, L. R. Hargreaves *et al.*, J. Phys. B: At., Mol. Opt. Phys. **46**, 125201 (2013).
[12] L. Hargreaves, K. Ralphs, G. Serna *et al.*, J. Phys. B: At., Mol. Opt. Phys. **45**, 201001 (2012).
[13] P. A. Thorn, M. J. Brunger, P. J. O. Teubner *et al.*, J. Chem. Phys. **126**, 064306 (2007).
[14] E. N. Lassettre and A. Skerbele, J. Chem. Phys. **60**, 2464 (1974).
[15] M. Matsui, M. Hoshino, H. Kato *et al.*, Eur. Phys. J. D **70**, 77 (2016); M. J. Brunger, P. A. Thorn, L. Campbell *et al.*, Int. J. Mass Spectrom. **271**, 80 (2008); P. A. Thorn, M. J. Brunger, H. Kato *et al.*, J. Phys. B: At., Mol. Opt. Phys. **40**, 697 (2007); K. N. Klump and E. N. Lassettre, Can. J. Phys. **53**, 1825 (1975); E. N. Lassettre and E. R. White, J. Chem. Phys. **60**, 2460 (1974); S. Trajmar, W. Williams, and A. Kuppermann, *ibid.* **58**, 2521 (1973); S. R. Mielczarek and K. J. Miller, Chem. Phys. Lett. **10**, 369 (1971).
[16] N. Durante, U. T. Lamanna, G. P. Arrighini *et al.*, Theor. Chim. Acta **90**, 115 (1995).
[17] T. N. Rescigno and A. E. Orel, Phys. Rev. A **88**, 012703 (2013); J. D. Gorfinkiel, L. A. Morgan, and J. Tennyson, J. Phys. B: At., Mol. Opt. Phys. **35**, 543 (2002); L. A. Morgan, *ibid.* **31**, 5003 (1998); M.-T. Lee, S. E. Michelin, T. Kroin *et al.*, *ibid.* **28**, 1859 (1995); M.-T. Lee, S. E. Michelin, L. E. Machado *et al.*, *ibid.* **26**, L203 (1993); T. J. Gil, T. N. Rescigno, C. W. McCurdy, and B. H. Lengsfield, Phys. Rev. A **49**, 2642 (1994); L. Chantranupong, G. Hirsch, R. J. Buenker *et al.*, Chem. Phys. **154**, 13 (1991); H. P. Pritchard, V. McKoy, and M. A. P. Lima, Phys. Rev. A **41**, 546(R) (1990); K. Bhanuprakash, P. Chandra, C. Chabalowski *et al.*, Chem. Phys. **138**, 215 (1989); K. J. Miller, S. R. Mielczarek, and M. Krauss, J. Chem. Phys. **51**, 26 (1969).
[18] R. Mota, R. Parafita, A. Giuliani *et al.*, Chem. Phys. Lett. **416**, 152 (2005).
[19] J. Berkowitz, *Atomic and Molecular Photoabsorption: Absolute Total Cross Sections*, 1st ed. (Academic, London, 2001).
[20] L. C. Lee and M. Suto, Chem. Phys. **110**, 161 (1986).
[21] P. L. Smith, K. Yoshino, H. E. Griesinger, and J. H. Black, Astrophys. J. **250**, 166 (1981).
[22] A. Rauk and J. B. Barriel, Chem. Phys. **25**, 409 (1977).
[23] R. J. Buenker and S. D. Peyerimhoff, Chem. Phys. Lett. **29**, 253 (1974).
[24] P. Gürtler, V. Saile, and E. E. Koch, Chem. Phys. Lett. **51**, 386 (1977).
[25] W. F. Chan, G. Cooper, and C. E. Brion, Chem. Phys. **178**, 387 (1993).
[26] G. J. Kutcher and A. E. S. Green, Radiat. Res. **67**, 408 (1976).
[27] J. J. Olivero, R. W. Stagat, and A. E. S. Green, J. Geophys. Res. **77**, 4797 (1972).
[28] X. J. Liu, L. F. Zhu, X. M. Jiang *et al.*, Rev. Sci. Instrum. **72**, 3357 (2001).
[29] J. C. Nickel, P. W. Zetner, G. Shen *et al.*, J. Phys. E: Sci. Instrum. **22**, 730 (1989); Y. W. Liu, L. Q. Xu, D. D. Ni *et al.*, J. Geophys. Res. Space Phys. **122**, 3459 (2017).

[30] K. Z. Xu, R. F. Feng, S. L. Wu, Q. Ji, X. J. Zhang, Z. P. Zhong, and Y. Zheng, Phys. Rev. A **53**, 3081 (1996); N. M. Cann and A. J. Thakkar, J. Electron. Spectrosc. Relat. Phenom. **123**, 143 (2002); X. Y. Han and J. M. Li, Phys. Rev. A **74**, 062711 (2006); B. P. Xie, L. F. Zhu, K. Yang, B. Zhou, N. Hiraoka, Y. Q. Cai, Y. Yao, C. Q. Wu, E. L. Wang, and D. L. Feng, *ibid.* **82**, 032501 (2010)..

[31] W. A. Goddard III and W. J. Hunt, Chem. Phys. Lett. **24**, 464 (1974).

[32] H.-t. Wang, W. S. Felps, and S. P. McGlynn, J. Chem. Phys. **67**, 2614 (1977).

[33] E. N. Lassettre, J. Chem. Phys. **43**, 4479 (1965).

[34] K. N. Klump and E. N. Lassettre, J. Chem. Phys. **68**, 886 (1978).

[35] A. R. P. Rau and U. Fano, Phys. Rev. **162**, 68 (1967).

[36] L. Vriens, Phys. Rev. **160**, 100 (1967); Y. K. Kim, J. Chem. Phys. **126**, 064305 (2007), and references therein.

[37] H. Kawahara, D. Suzuki, H. Kato, M. Hoshino, and H. Tanaka, J. Chem. Phys. **131**, 114307 (2009); Y. Y. Wang, J. M. Sun, and L. F. Zhu, *ibid.* **132**, 124301 (2010); Y.-W. Liu, L.-Q. Xu, T. Chen, D.-G. Qi, T. Xiong, and L.-F. Zhu, Astrophys. J., Suppl. Ser. **234**, 10 (2018); X. Xu, L.-Q. Xu, T. Xiong, T. Chen, Y.-W. Liu, and L.-F. Zhu, J. Chem. Phys. **148**, 044311 (2018).

[38] Y. K. Kim, Phys. Rev. A **64**, 032713 (2001).

[39] R. J. Buenker, M. Honigmann, and H.-P. Liebermann, J. Chem. Phys. **113**, 1046 (2000); L.-Q. Xu, X. Kang, Y.-G. Peng, X. Xu, Y. W. Liu, Y. Wu, K. Yang, N. Hiraoka, K. D. Tsuei, J. G. Wang, and L. F. Zhu, Phys. Rev. A **97**, 032503 (2018).

[40] B. H. Bransden and C. J. Joachain, *Physics of Atoms and Molecules* (Prentice Hall, Harlow, UK, 2003); P. G. Burke, AIP Conf. Proc. **543**, 155 (2000).

[41] X. Hu, C.-Z. Gao, Z. Chen, J. Wang, Y. Wu, and Y. Wang, Phys. Rev. A **96**, 052701 (2017).

[42] T. H. Dunning, J. Chem. Phys. **90**, 1007 (1989).

[43] H.-J. Werner, P. J. Knowles, G. Knizia, F. R. Manby, and M. Schütz, WIREs Comput. Mol. Sci. **2**, 242 (2012); Q. Ma and H. Werner, *ibid.* **8**, e1371 (2018).

[44] R. J. Buenker and S. D. Peyerimhoff, Theor. Chim. Acta **35**, 33 (1974); *ibid.* **39**, 217 (1975); R. J. Buenker, S. D. Peyerimhoff, and W. Butscher, Mol. Phys. **35**, 771 (1978).